AIAA SciTech Forum
11–15 & 19–21 January 2021, VIRTUAL EVENT
AIAA Scitech 2021 Forum

10.2514/6.2021-0745

Time integration considerations for the solution of reacting flows using discontinuous Galerkin methods

Brett Bornhoft*, Eric Ching, and Matthias Ihme
Department of Mechanical Engineering, Stanford University
Stanford, CA 94305, United States

I. Abstract

In this work, we present intermediate steps to develop a discontinuous Galerkin (DG) discretization in both space and time applicable to multi-component reacting flows. Here, we choose the ADER time integration method for its compact stencil, arbitrary order of accuracy in space and time, and its ability to handle stiff source terms such as those present in reacting flows. In this paper, we verify the scheme for an isentropic vortex, assess its behavior for discontinuous properties, and compare the scheme to explicit methods under a simplified stiff source term. We conclude this paper by conducting a demonstration of an overdriven detonation with a single-step irreversible reaction mechanism.

II. Introduction

High-order discontinuous Galerkin (DG) methods have become more popular in recent years. This is largely due to several features that provide additional benefits over those of more traditional discretization approaches like finite-volume methods. Attractive features of DG methods include compact stencils and high-order accuracy on arbitrary mesh topologies. Compact stencils offer the benefit of reducing communication on highly-parallel simulations and are portable to modern computational architectures such as GPUs. Arbitrary mesh topologies can reduce the time to create a grid as well as relax restrictions on grid quality. However, despite its success, open research topics for DG methods remain such as shock-capturing techniques [1], particle-laden flows [2], multiphase flows [3], reacting flows [4, 5], and efficient time integration [6, 7].

For the current work, we focus on the application of time integration schemes in the context of multi-component reacting flows. The ability to solve systems of equations with stiff source terms efficiently and accurately is critical to computational combustion. DG methods have only seen minimal use in reacting flows. Efforts have already included application to turbulent reacting flows [8, 9], but these current studies have yet to show advantages over traditional finite-volume approaches [10, 11]. One reason for this is that DG methods are fairly restrictive on their time-step selection leading to high computational cost per a specified grid resolution. This is only exacerbated in reacting flows with highly stiff source terms.

In this work, we utilize a time integration technique that uses the DG framework to achieve high-order of accuracy in space and time while handling stiff source terms. The scheme first developed in the context of Riemann solvers for linear systems by Toro et al. [12] who utilized the Lax-Wendroff procedure to substitute temporal derivatives with a Taylor expansion of spatial derivatives using the governing conservation law in differential form. The scheme was coined *ADER*, an abbreviation for "**A**rbitrary high-order schemes using derivatives." According to Dumbser et al., methods based on Taylor series are not well suited for equations with stiff source terms [13]. Rather than relying on the Cauchy-Kovalewskaya procedure, Dumbser utilized the DG discretization itself where they enforced integraton by parts on the temporal integral instead of the flux integral. This scheme was first introduced in the context of finite volume schemes [13], but was later extended to DG methods with applications to stiff sources [14]. The method is cast as a predictor-corrector type scheme. First, a predicted space-time solution is found through a *weak* solution to our system of partial differential equations (PDEs), meaning we do not consider jump conditions through the interaction of neighbor elements. Then, we utilize the predicted solution vector to advance our solution in time through a DG discretization in space-time.

In the present study, several intermediate steps are taken to extend the ADER-DG method to applications of finite-rate chemically reacting flows. To the authors' knowledge, the ADER scheme has only been applied to finite-rate chemistry within the context of finite-volume schemes [15]. ADER-DG has several attractive features that suggest it has the potential to rival state-of-the-practice operator splitting schemes [16, 17]. While operator-splitting schemes are restricted

*bornhoft@stanford.edu

to second order accuracy in time, the ADER-DG approach can achieve arbitrary orders of accuracy in both space and time. In addition, due to the space-time polynomial expansion, it is possible to use local time-stepping in a conservative sense where time-accuracy can be ensured [18].

The remainder of the work will follow the proposed structure. Section III introduces the governing equations and the ADER-DG discretization. Special attention will be made regarding the predictor portion as it pertains to stiff systems. Section IV will provide results and discuss the performance of the scheme for various applications. In this section, we will verify the schemes order of accuracy and assess its performance on two discontinuous flow fields. We will discuss and illustrate the benefits of ADER-DG in the stiff limit. Lastly, we will conduct an exploratory case where we simulate an overdriven detonation. In Section V, conclusions and future work will be discussed.

III. Mathematical formulation

This section describes the governing equations and the details of the DG method.

A. Governing equations

The behavior of the reacting gas is described by the compressible multi-component Euler equations, written in vector form as

$$\partial_t \boldsymbol{U} + \nabla \cdot \boldsymbol{F}_c = \boldsymbol{S}, \tag{1}$$

where $\boldsymbol{U}(\boldsymbol{x}, t) : \mathbb{R}^{N_d} \times \mathbb{R}^+ \rightarrow \mathbb{R}^{N_U}$ is the conservative state vector, $\boldsymbol{F}_c(\boldsymbol{U}) : \mathbb{R}^{N_U} \rightarrow \mathbb{R}^{N_U \times N_d}$ is the inviscid flux vector, and $\boldsymbol{S}(\boldsymbol{U}) : \mathbb{R}^{N_d} \times \mathbb{R}^+ \rightarrow \mathbb{R}^{N_U}$ is the source term vector. In addition, $\boldsymbol{x} \in \mathbb{R}^{N_d}$ is the spatial coordinate vector, $t \in \mathbb{R}^+$ is the time, N_U is the number of state variables, and N_d is the number of spatial dimensions. The terms in Eq. (1) can be expanded as

$$\boldsymbol{U} = \begin{bmatrix} \rho \\ \rho \boldsymbol{u} \\ \rho E \\ \rho Y_1 \\ \vdots \\ \rho Y_{N_S-1} \end{bmatrix}, \quad \boldsymbol{F}_c = \begin{bmatrix} \rho \boldsymbol{u}^T \\ \rho \boldsymbol{u} \otimes \boldsymbol{u} + P\mathbb{I} \\ (\rho E + P)\boldsymbol{u}^T \\ \rho Y_1 \boldsymbol{u}^T \\ \vdots \\ \rho Y_{N_s-1} \boldsymbol{u}^T \end{bmatrix}, \quad \boldsymbol{S} = \begin{bmatrix} 0 \\ 0 \\ \dot{\omega}_T \\ \dot{\omega}_1 \\ \vdots \\ \dot{\omega}_{N_S-1} \end{bmatrix}, \tag{2}$$

where ρ is the fluid density, $\boldsymbol{u}$ is the velocity vector, P is the pressure, E is the total non-chemical energy per unit mass, Y_k is the mass fraction of species k, and $\mathbb{I}$ is the identity matrix.

The heat flux vector can be written as

$$\boldsymbol{q} = -k\nabla T + \rho \sum_k h_{s,k} Y_k \boldsymbol{V}_k \tag{3}$$

where k is the thermal conductivity and $h_{s,k}$ is the species sensible ethalpy. The enthalpy of species k can be written as

$$h_k = \Delta h^0_{f,k}(T_{\text{ref}}) + \int_{T_{\text{ref}}}^{T} c_{p,k}(T) dT \tag{4}$$

where $\Delta h^0_{f,k}(T_{\text{ref}})$ is the formation enthalpy at the reference temperature of 298.15 K and $c_{p,k}(T)$ is the temperature dependent heat capacity both for species k.

For the preliminary results we consider single-component gases and limit our cases to sources that can be used to represent the stiffness present in chemically reacting flows. Previous efforts by Bando et al. [5] showed the capability to simulate multi-component reacting flows, but here the focus of this work pertains to the application of the ADER-DG scheme to these equations and as such we choose to start with the simplified set of Euler equations with a stiff source term.

B. Discontinuous Galerkin Discretization

Let Ω denote the computational domain, which is partitioned into N_e non-overlapping discrete elements such that $\Omega = \cup_{e=1}^{N_e} \Omega_e$. $\partial\Omega_e$ is the boundary of element Ω_e. The space of test functions is defined as

$$\mathcal{V}_h^p = \{\phi \in L^2(\Omega), \phi|_{\Omega_e} \in \mathcal{P}_p(\Omega_e) \; \forall \; \Omega_e \in \Omega\}, \tag{5}$$

where ϕ is the test function and $\mathcal{P}_p$ denotes the space of polynomial functions of degree no greater than p. The approximation to the global solution, $\boldsymbol{U}_h \simeq \boldsymbol{U}$, can be expanded as

$$\boldsymbol{U}_h = \oplus_{e=1}^{N_e} \boldsymbol{U}_h^e, \tag{6}$$

where $\boldsymbol{U}_h^e$ is the local discrete solution,

$$\boldsymbol{U}_h^e(\boldsymbol{x}, t) = \sum_{n=1}^{N_b} \boldsymbol{U}_n^e(t)\phi_n(\boldsymbol{x}), \tag{7}$$

$\boldsymbol{U}_n^e(t) : \mathbb{R}^+ \rightarrow \mathbb{R}^{N_U}$ is the nth vector of basis coefficients, and $\{\phi_n\}_{\{n=1,\ldots,N_b\}}$ is a basis of $\mathcal{P}_p(\Omega_e)$, chosen in this work to be a Lagrange polynomial basis.

To solve for the local discrete solution, we multiply the governing PDE system in Eq. (1) by the basis and integrate over a space-time control volume $\Omega_e \times [t_n, t_{n+1}]$. This leads to

$$\int_{t_n}^{t_{n+1}} \int_{\Omega_e} \phi_m \partial_t \boldsymbol{U}_h^e d\Omega dt + \int_{t_n}^{t_{n+1}} \int_{\Omega_e} \phi_m \nabla \cdot \boldsymbol{F}_c(\boldsymbol{U}_h^e) d\Omega dt = \int_{t_n}^{t_{n+1}} \int_{\Omega_e} \phi_m \boldsymbol{S}(\boldsymbol{U}_h^e) d\Omega dt \; \forall \; \phi_m. \tag{8}$$

In a traditional DG discretization, Eq. (8) would not be integrated in time and temporal integration would be conducted through Runge-Kutta type schemes. Under this approach, the convective flux integral would be expressed through integration by parts where jump conditions would be incorporated from the nearest neighbors of each element. This forces additional communication at each stage of the Runge-Kutta solver due to the information required to solve these jump conditions. For ADER-DG, higher-order accuracy in time is not achieved through multiple stages but rather through an element local space-time predictor solution. This predictor step, described in Section (1) below, is arguably the most important step in the ADER-DG scheme.

1. Space-Time Predictor Step

We introduce the element local space-time predictor solution as

$$\boldsymbol{q}_h^e(\boldsymbol{x}, t) = \sum_k \psi_k(\boldsymbol{\xi}, \tau) \widetilde{\boldsymbol{q}}_k^e \tag{9}$$

to represent the predictor solution of our space-time element. We note that $\boldsymbol{q}_h^e(\boldsymbol{x}, t^n) = \boldsymbol{U}_h^e(\boldsymbol{x})$. The set of basis functions $\{\psi_k\}_{k=1,\ldots,N_b^{st}}$ are constructed using tensor products of the one dimensional basis (here chosen to be Lagrange polynomials). To solve for this local discrete solution, we require $\boldsymbol{q}_h^e$ to satisfy Eq. (8). Therefore, our equation governing the predicted solution is as follows

$$\int_{t_n}^{t_{n+1}} \int_{\Omega_e} \psi_k \partial_t \boldsymbol{q}_h^e d\Omega dt + \int_{t_n}^{t_{n+1}} \int_{\Omega_e} \psi_k \nabla \cdot \boldsymbol{F}(\boldsymbol{q}_h^e) d\Omega dt = \int_{t_n}^{t_{n+1}} \int_{\Omega_e} \psi_k \boldsymbol{S}(\boldsymbol{q}_h^e) d\Omega dt \; \forall \; \psi_k. \tag{10}$$

At this point, rather than integrating the convective flux term by parts, we instead integrate the first term in Eq. (10) by parts. This leads to

$$\begin{aligned} \int_{\Omega_e} \psi_k \boldsymbol{q}_h^e d\Omega|_{t_{n+1}} - \int_{\Omega_e} \psi_k \boldsymbol{U}_h^e d\Omega|_{t_n} - \int_{t_n}^{t_{n+1}} \int_{\Omega_e} \frac{\partial \psi_k}{\partial t} \boldsymbol{q}_h^e d\Omega dt \\ + \int_{t_n}^{t_{n+1}} \int_{\Omega_e} \psi_k \nabla \cdot \boldsymbol{F}(\boldsymbol{q}_h^e) d\Omega dt = \int_{t_n}^{t_{n+1}} \int_{\Omega_e} \psi_k \boldsymbol{S}(\boldsymbol{q}_h^e) d\Omega dt \end{aligned} \tag{11}$$

The first two terms in Eq. (11) can be thought of as an upwind temporal flux where the solution $\boldsymbol{U}_h^e(\boldsymbol{x}, t_n)$ is known. Next, the polynomial representations of $\boldsymbol{q}_h^e$ and $\boldsymbol{U}_h^e$ are substituted into Eq. (11) and we recast our integrals in reference space. We define our reference coordinates in space-time to be $\boldsymbol{\xi}, \tau$ respectively where $-1 \leq \boldsymbol{\xi} \leq 1$ and $-1 \leq \tau \leq 1$ and $\Omega_e^{st} \in \mathbb{R}^{N_d+1}$. Changing to reference space gives us

$$\begin{aligned} \int_{\xi} \psi_k \psi_l d\boldsymbol{\xi} \widetilde{\boldsymbol{q}}_l^e|_{\tau=1} - \int_{\xi} \psi_k \phi_m d\boldsymbol{\xi} \widetilde{\boldsymbol{U}}_m^e|_{\tau=-1} - \int_{-1}^{1} \int_{\xi} \frac{\partial \psi_k}{\partial \tau} \psi_l d\boldsymbol{\xi} d\tau \widetilde{\boldsymbol{q}}_l^e \\ + \frac{\Delta t}{2} \int_{-1}^{1} \int_{\xi} \psi_k \nabla_{\xi} \cdot \boldsymbol{F}(\psi_l \widetilde{\boldsymbol{q}}_l^e) \boldsymbol{J}_e^{-T} d\boldsymbol{\xi} d\tau = \frac{\Delta t}{2} \int_{-1}^{1} \int_{\xi} \psi_k \boldsymbol{S}(\psi_l \widetilde{\boldsymbol{q}}_l^e) d\boldsymbol{\xi} d\tau, \end{aligned} \tag{12}$$

where, for brevity, we rely on index notation to imply summing over repeated indices.

We choose to represent the flux and source terms as polynomials with the same form as in Eq. (9).

$$\mathcal{F}_h^{*e}(\boldsymbol{\xi},\tau) = \sum_k \psi_k(\boldsymbol{\xi},\tau)\boldsymbol{F}_k^{*e} \tag{13}$$

$$\mathcal{S}_h^{*e}(\boldsymbol{\xi},\tau) = \sum_k \psi_k(\boldsymbol{\xi},\tau)\boldsymbol{S}_k^{*e} \tag{14}$$

where $\boldsymbol{F}^* = \boldsymbol{F}\frac{\Delta t}{2}$ and $\boldsymbol{S}^* = \boldsymbol{S}\frac{\Delta t}{2}$. This then leads to the following equation for $\widetilde{\boldsymbol{q}}_h^e$.

$$\begin{aligned}\underbrace{\left(\int_\xi \psi_k\psi_l d\boldsymbol{\xi}|_{\tau=1} - \int_{-1}^{1}\int_\xi \frac{\partial\psi_k}{\partial\tau}\psi_l d\boldsymbol{\xi}d\tau\right)}_{\boldsymbol{K}}\widetilde{\boldsymbol{q}}_l^e = &\underbrace{\int_\xi \psi_k\phi_m d\boldsymbol{\xi}|_{\tau=-1}}_{\boldsymbol{F_o}}\widetilde{\boldsymbol{U}}_m^e \\ &- \underbrace{\int_{-1}^{1}\int_\xi \psi_k\nabla_{\boldsymbol{x}}\psi_l d\boldsymbol{\xi}d\tau}_{\boldsymbol{K}_{\boldsymbol{x}}^e}\cdot\mathcal{F}_h^{*e} + \underbrace{\int_{-1}^{1}\int_\xi \psi_k\psi_l d\boldsymbol{\xi}d\tau}_{\boldsymbol{M}^{st}}\mathcal{S}_h^{*e}\end{aligned} \tag{15}$$

This is a local non-linear equation for the predicted solution vector in space-time that requires no knowledge of any neighboring elements. We solve this system using a fixed-point Picard iteration approach where

$$\widetilde{\boldsymbol{q}}_l^{n+1} = \boldsymbol{K}^{-1}\left(\boldsymbol{F}_o\boldsymbol{U}_m^e - \boldsymbol{K}_{\boldsymbol{x}}^e\mathcal{F}_l^{*e}(\widetilde{\boldsymbol{q}}_l^n) + \boldsymbol{M}^{st}\mathcal{S}_l^{*e}(\widetilde{\boldsymbol{q}}_l^n)\right) \tag{16}$$

In the case of stiff source terms, Eq. (16) is not entirely sufficient. To account for the stiffness, we take the source term coefficients implicitly such that

$$\widetilde{\boldsymbol{q}}_l^{n+1} - \boldsymbol{K}^{-1}\boldsymbol{M}^{st}\mathcal{S}_l^{*e}(\widetilde{\boldsymbol{q}}_l^{n+1}) = \boldsymbol{K}^{-1}\left(\boldsymbol{F}_o\widetilde{\boldsymbol{U}}_m^e - \boldsymbol{K}_{\boldsymbol{x}}^e\mathcal{F}_l^{*e}(\widetilde{\boldsymbol{q}}_l^n)\right). \tag{17}$$

The source term is then represented using a simple linearization:

$$\mathcal{S}_l^{*e,n+1} \approx \mathcal{S}_l^{*e,n} + \Delta t\left(\widetilde{\boldsymbol{q}}_l^{n+1} - \widetilde{\boldsymbol{q}}_l^n\right)\left(\frac{\partial\boldsymbol{S}}{\partial\boldsymbol{U}}\right)\Big|_{\bar{U}}^T \tag{18}$$

After substituting Eq. (18) into Eq. (17) we can cast the iterative approach in the following way

$$\underbrace{\left(\frac{(\boldsymbol{M}^{st})^{-1}\boldsymbol{K}}{\Delta t}\right)}_{\boldsymbol{A}}\widetilde{\boldsymbol{q}}_l^{n+1} + \widetilde{\boldsymbol{q}}_l^{n+1}\underbrace{\left(-\frac{\partial\boldsymbol{S}}{\partial\boldsymbol{U}}\right)\Big|_{\bar{U}}^T}_{\boldsymbol{B}} = \underbrace{\frac{1}{\Delta t}\mathcal{S}_l^{*e,n} - \widetilde{\boldsymbol{q}}_l^n\left(\frac{\partial\boldsymbol{S}}{\partial\boldsymbol{U}}\right)\Big|_{\bar{U}}^T + \frac{(\boldsymbol{M}^{st})^{-1}}{\Delta t}\left(\boldsymbol{F}_o\widetilde{\boldsymbol{U}}_m^e - \boldsymbol{K}_{\boldsymbol{x}}^e\mathcal{F}_l^{*e}(\widetilde{\boldsymbol{q}}_l^n)\right)}_{\boldsymbol{C}} \tag{19}$$

In this form, our local nonlinear solver is known as the Sylvester equation, which we solve iteratively [19].

2. Space-Time Correction Step

The polynomial representation of the space-time solution vector is then substituted into Eq. (8) followed by integration by parts of the flux function's term. Therefore, our correction step becomes

$$\begin{aligned}\left(\int_{\Omega_e}\phi_m\phi_k d\Omega\right)\left(\tilde{\boldsymbol{U}}_m^{e,n+1} - \tilde{\boldsymbol{U}}_m^{e,n}\right) - \int_{t_n}^{t_{n+1}}\int_{\Omega_e}\nabla\phi_m\cdot\boldsymbol{F}(\boldsymbol{q}_h^e)d\Omega dt \\ + \int_{t_n}^{t_{n+1}}\oint_{\partial\Omega_e}\phi_m\widehat{\boldsymbol{F}}(\boldsymbol{q}_h^{e+},\boldsymbol{q}_h^{e-},\widehat{\boldsymbol{n}})d\Gamma dt = \int_{t_n}^{t_{n+1}}\int_{\Omega_e}\phi_m\boldsymbol{S}(\boldsymbol{q}_h^e)d\Omega dt\end{aligned} \tag{20}$$

Here, the jump conditions between element neighbors are taken into consideration via a numerical flux function. Any limiting that is applied is done so at the end of the space-time correction step. To maintain stability for sharp discontinuities such as shocks we utilize two different limiters in this work. First, we use the positivity-preserving

limiter (PPL) from [20], which does not guarantee positivity for the ADER-DG approach given that it is not a convex combination of the Euler method. Even still, it provides additional robustness to our method. Second, we apply the WENO limiter of Zhong and Shu [21]. This limiter uses a TVB modified minmod function as a troubled cell indicator [22] where the free parameter M can be utilized to increase the limiting in the solution by increasing the number of troubled elements. The local solution for each troubled element is then reconstructed via a convex combination of the solution state of the element and its neighbors. The left and right eigenvectors (as derived in [23] for both reacting and non-reacting Euler equations) of the flux Jacobian are used to transform the solution into and out of the characteristic space. This convex combination occurs in characteristic space using the WENO procedure defined in [21].

IV. Results

In the following sections we outline the results of implementing the ADER-DG scheme into our current framework. The first is a convergence study across multiple orders of accuracy for a propagating vortex in two dimensions. We then show results of shock-tube and shock-density interaction problems to illustrate the sensitivity of the solution to the WENO limiter. The third is a brief discussion on the scheme's handling of stiff sources given a stiff friction term in the one dimensional Euler equations.Lastly, we present results of an overdriven detonation with finite-rate chemistry.

A. Convergence study of the 2D ADER-DG Implementation

The first case we choose to solve is a propagating vortex governed by Eq. (1). This is a classical case for testing the order of accuracy of higher-order schemes. In Figure 1 we show an example of the vortex on a square domain ranging from $[-5, 5]$ in both x- and y-directions. The vortex test case was adopted based on the work of Yu et al. [24] where the initial conditions are determined through the superposition of velocity and temperature perturbations onto a uniform flow. The perturbations are defined such that the entropy remains constant throughout the domain. Therefore, the exact solution to the propagating Gaussian wave is an advected Gaussian wave of the same magnitude. Here, we select our t_f = 0.5 s.

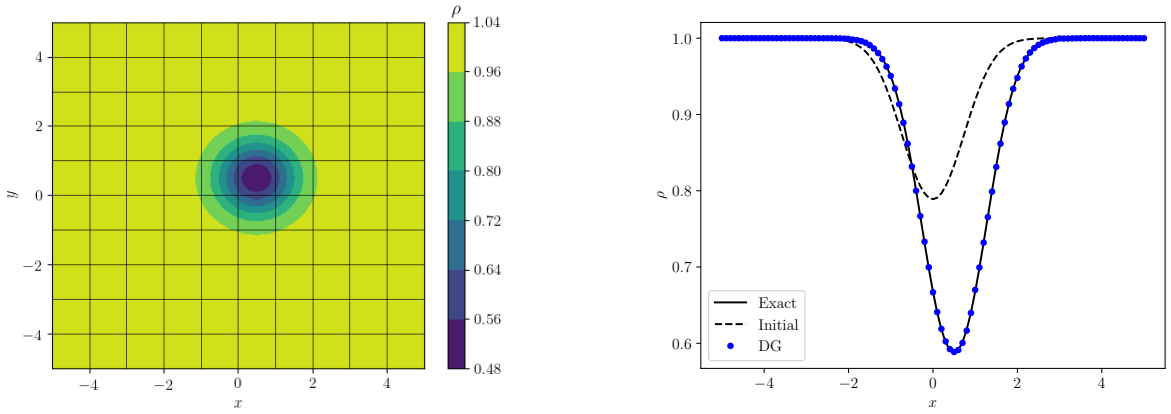

(a) Gaussian profiles

(b) Polynomial profiles

Fig. 1 (a) Density contours of the propagating vortex and (b) density line slices taken at $y = 1$.

In Table 1 we show the computational results obtained from propagating the vortex for 0.5 s. In each case we report the number of elements (N^e), degrees of freedom, (DOF), the L_2 error norm ($||e||_{L_2}$), and the order of convergence (O_{L_2}). We note that for all cases, the desired order of accuracy is achieved once the number of elements is sufficient to produce an error that is within the asymptotic limit of convergence. These h and p refinement studies verify that we are obtaining the expected order of accuracy for the given scheme.

B. Assessing capabilities for resolving discontinuities

In the following sections, we evaluate ADER-DG's ability to resolve discontinuities. This is critical as shock discontinuities are present in detonating flows.

N^e	$p = 1$ ADER-DG			$p = 2$ ADER-DG			$p = 3$ ADER-DG		
	DOF	$\|\|e\|\|_{L_2}$	O_{L_2}	DOF	$\|\|e\|\|_{L_2}$	O_{L_2}	DOF	$\|\|e\|\|_{L_2}$	O_{L_2}
25	100	2.89E-02		225	1.02E-02		400	2.46E-03	
100	400	1.07E-02	1.44	900	1.64E-03	2.64	1600	2.41E-04	3.35
400	1600	2.23E-03	2.26	3600	2.03E-04	3.01	6400	1.45E-05	4.06
1600	6400	4.27E-04	2.38	14400	2.40E-05	3.08	25600	9.09E-07	3.99
6400	25600	1.27E-04	1.75	57600	2.86E-06	3.07	102400	5.61E-08	4.02

Table 1 Convergence test of 2D vortex propagation across multiple orders of accuracy.

1. Sod Shock-tube

In this section, we consider the classic Sod shock-tube setup [25]. We use this case to evaluate the WENO limiter and the sensitivity of our solution to the TVB parameter (M). The one dimensional mesh has 100 elements and is on a domain from $[-5, 5]$. The initial conditions of the Sod problem are discontinuous flow properties at $x = 0$. The left and right states of the primitive variables are defined as:

$$(\rho, u, p) = \begin{cases} (1.0, 0.0, 0.0)^T & \text{if} \quad x \leq 0.0, \\ (0.125, 0.0, 0.1)^T & \text{if} \quad x > 0.0. \end{cases} \tag{21}$$

In Figures 2 and 3, numerical results are compared to the exact solution of the Riemann problem. For Figure 2, a TVB parameter of $M = 0.01$ is used. This decreases the threshold requirement for the shock indicator and therefore increases the amount of WENO limiting in the solution. In 2 (a) and (b), smooth regions at both the contact and shock locations indicate the application of the WENO limiter. Similar results are observed for both $p = 1$ and $p = 2$ solutions. In Figure 3, $M = 30.0$, which yields sharper results. We observe only small over and undershoots. In Figure 3 (b), both contact and shock discontinuities maintain their sharpness.

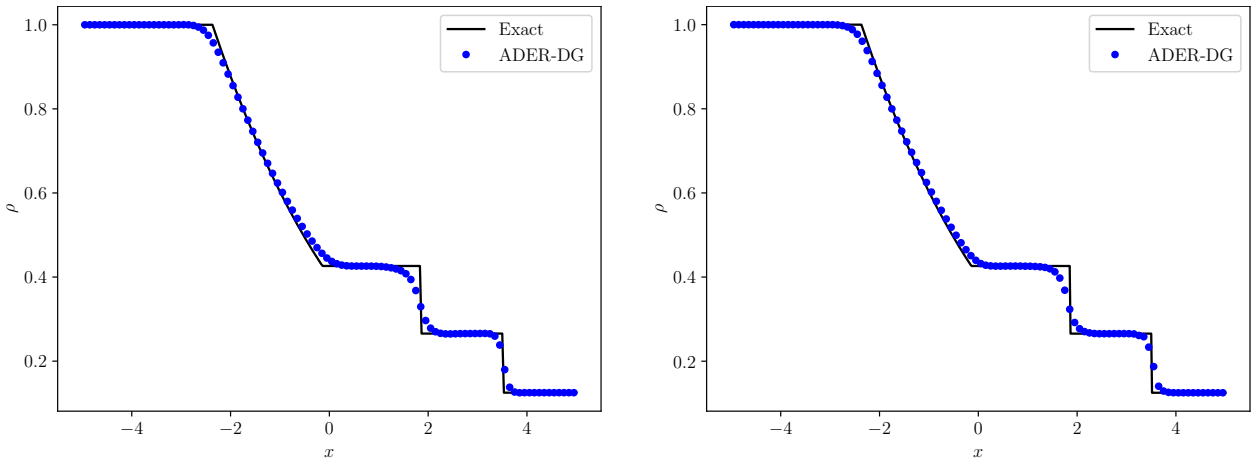

(a) $p = 1$, $M = 0.01$ (b) $p = 2$, $M = 0.01$

Fig. 2 Exact and numerical solution of the Sod shock tube problem at $t = 2$ with 100 elements and $M = 0.01$ (single point plotted per element).

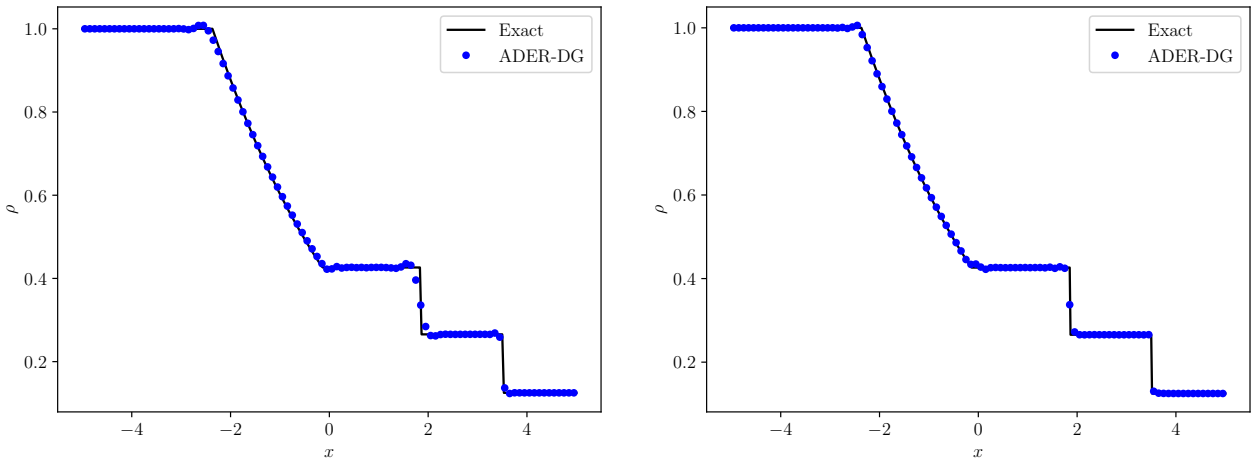

(a) $p = 1$, $M = 30.0$ (b) $p = 2$, $M = 30.0$

Fig. 3 Exact and numerical solution of the Sod shock tube problem at $t = 2$ with 100 elements and $M = 30.0$ (single point plotted per element).

2. Shock-density interaction

The shock-density interaction case first proposed by Shu and Osher [26] can be used to show the benefits of higher-order methods. The following initial conditions are used with the Euler equations:

$$(\rho, u, p) = \begin{cases} (3.857143, 2.629369, 10.333333)^T & \text{if} \quad x < -4, \\ (1.0 + 0.2\sin(5x), 0, 1)^T & \text{if} \quad x \geq -4. \end{cases} \tag{22}$$

Our results are shown in Figures 4 and 5. The solid line is the reference solution, here taken to be the "exact" solution. The reference solution was obtained from a 12000 element DGP2 simulation. Here, we again look at the effect of the TVB parameter. As we increase the parameter, and therefore decrease the amount of limiting, we obtain sharper results. In Figure 5 (b) we see that the scheme begins to resolve the minimum and maximum values of the density oscillations. The ADER-DGP1 case with $M = 100$ also required the use of the PPL. All other cases use only the WENO limiter.

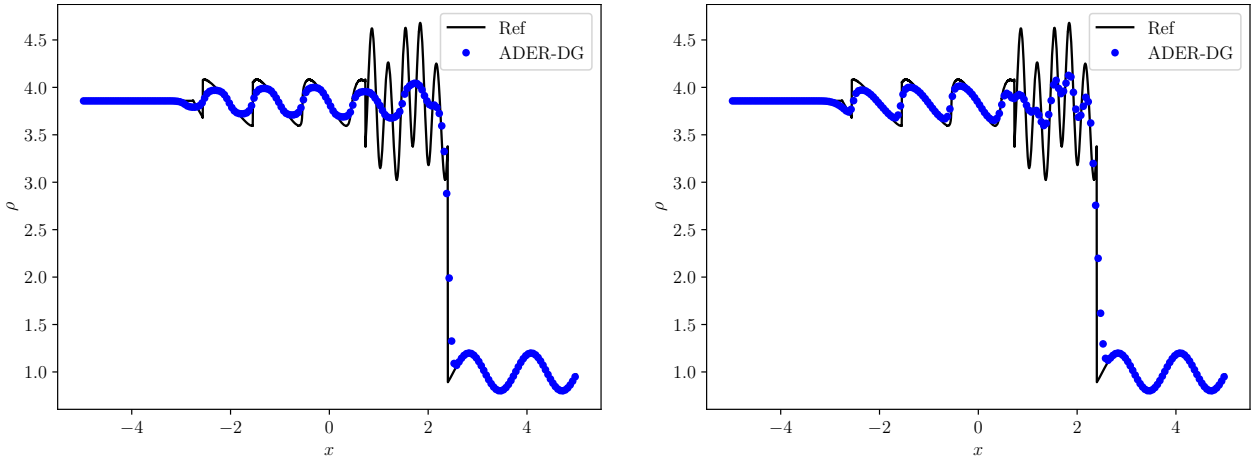

(a) $p = 1$, $M = 0.01$ (b) $p = 2$, $M = 0.01$

Fig. 4 Reference and numerical solution of the shock-density interaction at $t = 1.8$ with 200 elements and $M = 0.01$ (single point plotted per element).

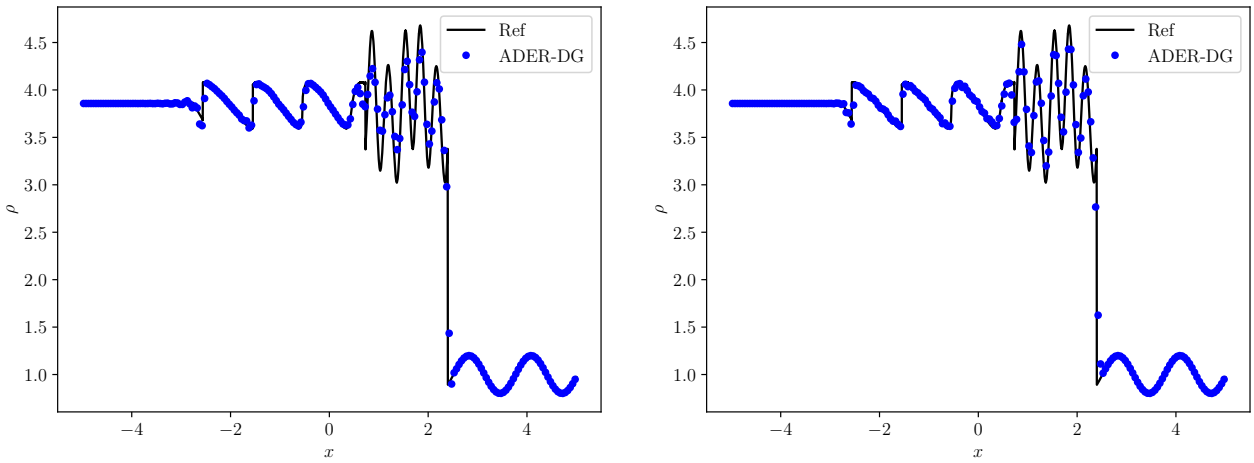

(a) $p = 1$, $M = 300$ (b) $p = 2$, $M = 300$

Fig. 5 Reference and numerical solution of the shock-density interaction at $t = 1.8$ with 200 elements and $M = 300$ (single point plotted per element).

C. Stiffness Considerations

Our primary purpose of utilizing the ADER discretization is to take advantage of its ability to handle stiff source terms. In this section, we detail a simplified example where we apply a non-linear source term modeling stiff friction that rapidly decays a propagating sine wave's momentum. The more rapid the decay occurs, the stiffer the system. We start with Eq. (1) and apply the following source term

$$\boldsymbol{S} = -\nu \begin{bmatrix} 0 \\ \rho \boldsymbol{u} \\ \rho \boldsymbol{u}^2 \end{bmatrix}, \tag{23}$$

The source models friction that acts proportional to the specified stiffness constant ν. The larger the value of ν the faster the system is brought to rest and the more stiffness is introduced into the equations. We consider the case in one dimension and use the following initial conditions in the computational domain $\Omega = [0; 1]$.

$$\begin{aligned} \rho(x, 0) &= 1 + 0.1 \sin(2\pi x), \\ u(x, 0) &= 1, \\ p(x, 0) &= 1. \end{aligned} \tag{24}$$

We specify $p = 3$ with 20 elements and run each case for $t = 0.5$ s, or half a period in the case of zero source. In Figure 6, we show an example of the final solution at $t_f = 0.5$ s. Here, we see that the momentum is zero and the energy converges to 2.5. We observe that the advection is slowed and less than half a period is made for the given time period. Our criteria for maximum allotted CFL number is whether or not the energy term, ρE, converges to this exact solution. For each ADER-DG case, we compare to an equivalent DG solution utilizing a 4^{th}-order Runge-Kutta scheme. In Table 2, the results of the CPU time for each case under a variety of stiffness values are considered. In the table, we use σ to represent the ratio of the wall clock time of the RK4-DG approach to the ADER-DG approach. In the absence of a stiff source term, the RK4-DG scheme is approximately twice as fast. There is extra cost in the local non-linear solve that occurs each iteration. As the stiffness parameter ν increases, the more cost effective the ADER-DG scheme becomes. This added benefit is from constructing the source term implicitly. In the very stiff case, we observe upwards of a 10x speed-up as compared to traditional explicit schemes. Under the stiff limit, the ADER-DG method out performs typical explicit schemes. This shows that it is a viable option for simulating reacting flows.

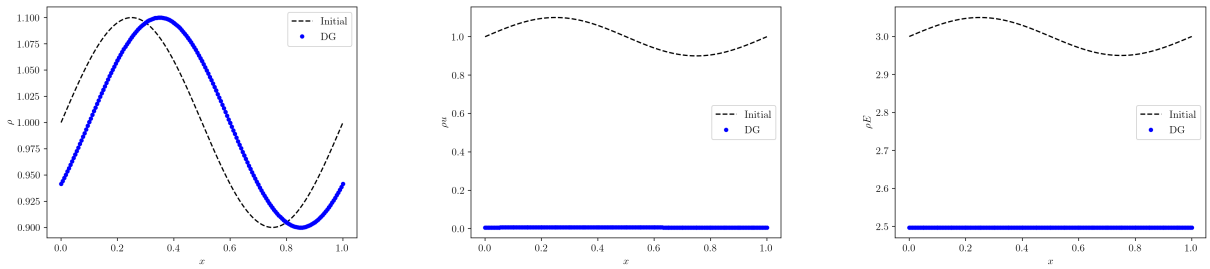

(a) Density (b) Momentum (c) Energy

Fig. 6 Example solution of stiff system using $p = 3$ on 20 elements with a $\nu = 10$.

ν	σ
100	0.54
500	1.73
1000	3.11
10000	10.04

Table 2 Wall clock time ratio comparison between RK4-DG and ADER-DG for a $p = 3$ solution to the Euler equation with various levels of stiffness.

D. Overdriven Detonation

The one dimensional overdriven detonation case is a temporally evolving unsteady wave. The gas mixture is considered calorically perfect with $\gamma = 1.2$ and $q = 50$ where

$$p = (\gamma - 1)\left(\rho E - \frac{1}{2}\rho u^2 - q\rho Y\right) \tag{25}$$

The chemical kinetics are governed by a single-step irreversible reaction where the reaction rate is described in the Arrhenius form.

$$\dot{\omega} = A\exp\left(-E_a/RT\right) \tag{26}$$

Here, we consider the nondimensional case where $R = 1$, $E_a = 50$, and $A = 230.75$. A single species mass fraction, Y, characterizes the conversion from the unburnt to burnt state for the single step chemistry. The initial conditions, which are characterized the same as in [27], are determined from the Zeldovich, Neumann, and Doering (ZND) profiles by specifying an overdrive factor, $\xi = 1.6$. Details of solving for the ZND initial condition can be found in Fickett and Davis [28]. We simulate a domain of $800L_{1/2}$, where $L_{1/2}$ is the distance required for half of the reactants to be consumed, here $L_{1/2} = 1.0$. The grid resolution is determined by the number of elements per $L_{1/2}$. In this study, we use $L_{1/2}/h = 20$. For this simulation, the WENO limiter is used with $M = 0.01$.

In Figure 7, numerical results showing both pressure and mass fraction profiles at $t = 60$s are plotted. A detonation front, here seen as a shock wave is followed by a reaction layer where the mass fraction is depleted. In Figure 7 (d), we observed that the reaction half length ($L_{1/2}$) is approximately one. This case follows a characteristic periodic behavior as observed in [27], [4], and [29]. In Figure 8, we see the maximum pressure, taken as the maximum pressure local to the detonation wave, as a function of time. Similar to Ref. [27], the maximum pressure converges to approximately 99. After a transient start up behavior we begin to observe the periodic behavior expected for the overdriven detonation. These promising results will continue to be vetted through parametric studies. In addition, the benefits of ADER-DG with respect to stiffness will be evaluated for a variety of detonation cases.

V. Conclusions and Future Work

In this paper we have shown how our implementation of the ADER-DG scheme represents an intermediate step towards solving stiff systems such as those observed in finite-rate chemically reacting flows. The scheme maintains the

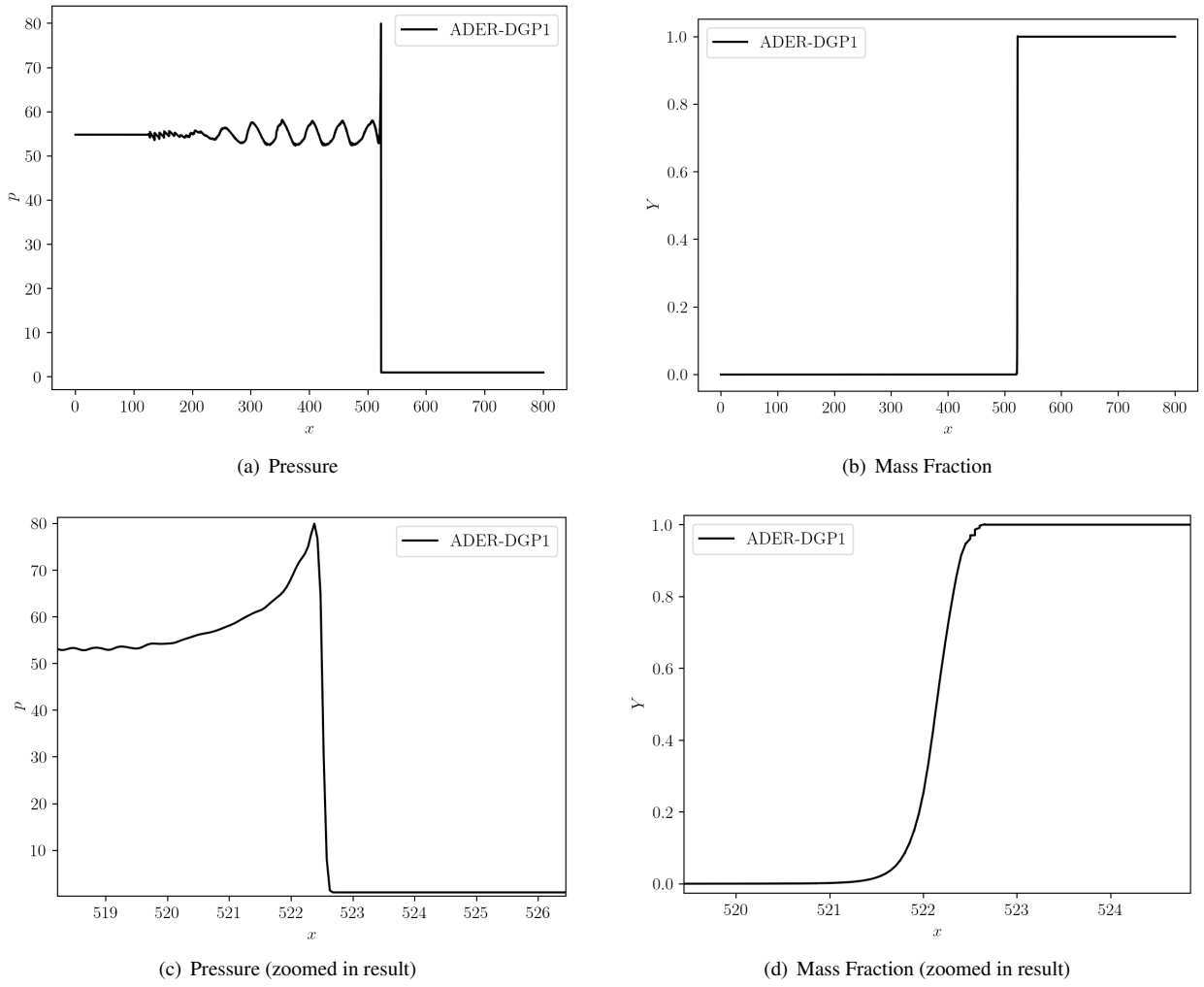

(a) Pressure

(b) Mass Fraction

(c) Pressure (zoomed in result)

(d) Mass Fraction (zoomed in result)

Fig. 7 ADER-DGP1 numerical results of the overdriven detonation at $t = 60$ showing (a) pressure, (b) mass fraction, (c) zoomed in pressure and (d) zoomed in mass fraction near the shock location (single point plotted per element).

expected order of accuracy in space and time while being able to handle stiff source terms. We showed that under the stiff limit, that the implicit treatment of the source term allows for a higher CFL number than typical explicit approaches. We applied PPL and WENO limiters to increase the robustness of the scheme. Lastly, we presented results of an overdriven detonation that demonstrates each separate components' utility in a more complex application. Based on the current ADER-DG implementation, it has been determined that the scheme shows promise when addressing stiff source terms such as those encountered in chemically reacting flows. Additional future work includes further parametric studies of the ADER-DG scheme and direct comparisons with other methods such as operator-splitting.

Acknowledgments

This work is supported by the DoD SMART Scholarship as well as through financial support through a NASA Early Career Faculty Award and NSF. This work used the Extreme Science and Engineering Discovery Environment (XSEDE), which is supported by National Science Foundation grant number ACI-1548562.

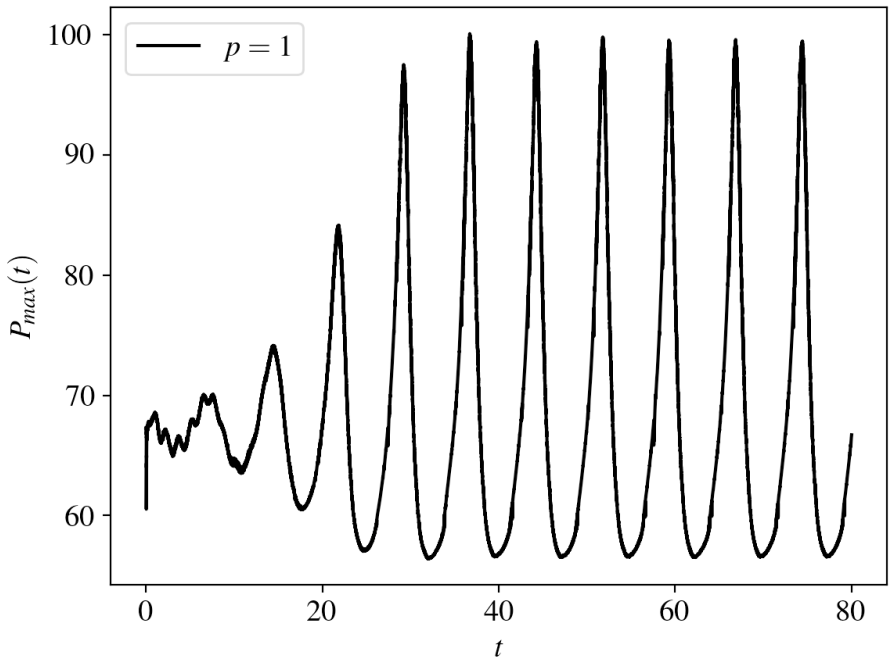

Fig. 8 Maximum pressure defined local to the detonation as a function of time.

References

[1] Ching, E. J., Lv, Y., Gnoffo, P., Barnhardt, M., and Ihme, M., "Shock capturing for discontinuous Galerkin methods with application to predicting heat transfer in hypersonic flows," *Journal of Computational Physics*, Vol. 376, 2019, pp. 54–75.

[2] Ching, E. J., Brill, S., Barnhardt, M., and Ihme, M., "A two-way-coupled Euler-Lagrange method for simulating multiphase flows with discontinuous Galerkin schemes on arbitrary curved elements," *Journal of Computational Physics*, Vol. 405, 2019.

[3] de Fraha, H., Varadan, M., and Johnsen, E., "A new limiting procedure for discontinuous Galerkin methods applied to compressible multiphase flows with shocks and interfaces," *Journal of Computational Physics*, Vol. 280, 2015, pp. 489–509.

[4] Lv, Y., and Ihme, M., "Discontinuous Galerkin method for multicomponent chemically reacting flows and combustion," *Journal of Computational Physics*, Vol. 270, 2014, pp. 105–137.

[5] Bando, K., Sekachev, M., and Ihme, M., "Comparison of algorithms for simulating multi-componentreacting flows using high-order discontinuous Galerkin methods," AIAA 2020-1751, Orlando, Florida, 2020.

[6] Froehle, B., and Persson, P.-O., "A high-order discontinuous Galerkin method for fluid–structure interaction with efficient implicit–explicit time stepping," *Journal of Computational Physics*, Vol. 272, 2014, pp. 455–470.

[7] Dumbser, M., Fambri, F., Tavelli, M., Bader, M., and Weinzierl, T., "Efficient Implementation of ADER Discontinuous Galerkin Schemes for a Scalable Hyperbolic PDE Engine," *Axioms*, Vol. 7, 2018.

[8] Wu, H., Ma, P., Lv, Y., and Ihme, M., "MVP-Workshop Contribution: Modeling of Volvo bluff body flame experiment," AIAA 2017-1573, Grapevine, Texas, 2017.

[9] Johnson, R., Goodwin, G., Corrigan, A., Kercher, A., and Chelliah, H., "Discontinuous-Galerkin Simulations of Premixed Ethylene-Air Combustion in a Cavity Combustor," AIAA 2019-1444, San Diego, California, 2019.

[10] Hassan, E., Peterson, D., Walters, K., and E.A., L., "Dynamic Hybrid Reynolds-Averaged Navier-Stokes/Large-Eddy Simulation of a Supersonic Cavity: Chemistry Effects," *Journal of Propulsion and Power*, Vol. 35, No. 1, 2018.

[11] Gallagher, T., and Sankaran, V., "Affordable Explicitly Filtered Large-Eddy Simulation for Reacting Flows," *AIAA Journal*, Vol. 57, No. 2, 2019.

[12] Toro, E. F., Millington, R., and Nejad, L., "Towards very high order Godunov schemes," *Godunov Methods. Theory and Applications*, edited by E. Toro, Springer, 2001, pp. 905–938.

[13] Dumbser, M., Enaux, C., and Toro, E., "Finite volume schemes of very high order of accuracy for stiff hyperbolic balance laws," *Journal of Computational Physics*, Vol. 227, 2008, pp. 3971–4001.

[14] Dumbser, M., and Zanotti, O., "Very high order $P_N P_M$ schemes on unstructured meshes for the resistive relativistic MHD equations," *Journal of Computational Physics*, Vol. 228, 2009, pp. 6991–7006.

[15] Hidalgo, A., and Dumbser, M., "ADER Schemes for Nonlinear Systems of Stiff Advection-Diffusion-Reaction Equations," *JSC*, Vol. 48, 2011, pp. 173–189.

[16] LeVeque, R. J., *Finite volume methods for hyperbolic problems*, Cambridge: Cambridge University Press, 2002.

[17] Wu, H., Ma, P., and Ihme, M., "Efficient time-stepping techniques for simulating turbulent reactive flows with stiff chemistry," *Computer Physics Communications*, Vol. 243, 2019, pp. 81–96.

[18] Lörcher, F., Gassner, G., and Munz, C.-D., "An explicit discontinuous Galerkin scheme with local time-stepping for general unsteady diffusion equations," *Journal of Computational Physics*, Vol. 227, 2008, pp. 5649–5670.

[19] Bartels, R., and Stewart, G., "Solution of the matrix equation $\boldsymbol{AX} + \boldsymbol{XB} = \boldsymbol{C}$," *Communications of the ACM*, Vol. 15, 1972.

[20] Wang, C., Zhang, X., Shu, C.-W., and Ning, J., "Robust high order discontinuous Galerkin schemes for two-dimensional gaseous detonations," *Journal of Computational Physics*, Vol. 231, No. 2, 2012, pp. 653–665.

[21] Zhong, X., and Shu, C.-W., "A simple weighted essentially nonoscillatory limiter for Runge-Kutta discontinuous Galerkin methods," *Journal of Computational Physics*, Vol. 232, No. 1, 2013, p. 397,„1¤7415.

[22] Shu, C.-W., "TVB uniformly high-order schemes for conservation laws," *Mathematics of Computation*, Vol. 49, 1987, pp. 105–211.

[23] Fedkiw, R., "A survey of chemically reacting, compressible ows," Ph.D. Thesis, University of California Los Angeles, 1997.

[24] Yu, M., Wang, Z., and Liu, Y., "On the accuracy and efficiency of discontinuous Galerkin, spectral difference and correction procedure via reconstruction methods," *Journal of Computational Physics*, Vol. 259, 2014, pp. 70–95.

[25] Sod, G., "A survey of several finite difference methods for systems of nonlinear hyperbolic conservation laws," *JCP*, Vol. 27, 1978, p. 1–31.

[26] Shu, C.-W., and Osher, S., "Efficient implementation of essentially non-oscillatory shock capturing schemes II," *Journal of Computational Physics*, Vol. 83, 1989, pp. 32–78.

[27] Hwang, P., Fedkiw, R., Merriman, B., Aslam, T., Karagozian, A., and Osher, S., "Numerical resolution of pulsating detonation waves," *Combustion Theory and Modeling*, Vol. 4, 2000, pp. 217–240.

[28] Fickett, W., and Davis, W., *Detonation - Theory and Experiment*, Dover Publications, 2000.

[29] Papalexandris, M., Leonard, A., and Dimotakis, P., "Unsplit Schemes for Hyperbolic Conservation Laws with Source Terms in One Space Dimension," *Journal of Computational Physics*, Vol. 134, 1997, pp. 31–61.